HHS Public Access

Author manuscript

Cell Rep. Author manuscript; available in PMC 2025 April 21.

Published in final edited form as:

Cell Rep. 2025 March 25; 44(3): 115393. doi:10.1016/j.celrep.2025.115393.

BATF2 is a regulator of interferon-γ signaling in astrocytes during neuroinflammation

Rachel A. Tinkey[1,2], **Brandon C. Smith**[1], **Maria L. Habean**[1,3], **Jessica L. Williams**[1,4,*]

[1]Department of Neurosciences, Lerner Research Institute, Cleveland Clinic, Cleveland, OH 44195, USA

[2]School of Biomedical Sciences, Kent State University, Kent, OH 44240, USA

[3]Department of Neurosciences, Case Western Reserve University, Cleveland, OH 44106, USA

[4]Lead contact

SUMMARY

Astrocytic interferon (IFN)γ signaling is associated with reduced neuroinflammation; however, downstream effectors responsible for regulating this protection are unknown. Here, we identify an IFN-specific transcription factor, basic leucine zipper ATF-like transcription factor (BATF)2, that plays a key role in modulating the consequences of IFNγ signaling in astrocytes. Chromatin immunoprecipitation sequencing revealed that BATF2 binds and prevents the overexpression of IFN regulatory factor (IRF)1 and IRF1 targets such as caspase-1. We also show that *Batf2*$^{-/-}$ mice exhibit exacerbated clinical disease severity in a murine model of central nervous system autoimmunity and express increased astrocyte-specific IRF1 and caspase-1, suggesting an amplified IFN response *in vivo*. Additionally, we demonstrate that BATF2 is expressed primarily in astrocytes within multiple sclerosis lesions and that this expression is colocalized

*Correspondence: williaj39@ccf.org.

AUTHOR CONTRIBUTIONS

Conceptualization, R.A.T., B.C.S., and J.L.W.; data curation, R.A.T., B.C.S., M.L.H., and J.L.W.; formal analysis, R.A.T.; writing – original draft, R.A.T.; writing – review & editing, R.A.T. and J.L.W.; funding acquisition, J.L.W.

RESOURCE AVAILABILITY

Lead contact

Further information and requests for resources and reagents should be directed to and will be fulfilled by the lead contact, Jessica L. Williams (williaj39@ccf.org).

Materials availability

All biological resources, antibodies, cell lines, model organisms, and tools are available either through commercial sources or upon request from the lead contact. Further information and requests for resources and reagents listed in the key resources table should be directed to the lead contact.

Data and code availability

- The accession numbers to access RNA sequencing and ChIP sequencing data can be found in the key resources table.
- This paper does not report original code.
- Any additional information required to reanalyze the data reported here is available from the lead contact upon request.

DECLARATION OF INTERESTS

The authors declare no competing interests.

SUPPLEMENTAL INFORMATION

Supplemental information can be found online at https://doi.org/10.1016/j.celrep.2025.115393.

with IRF1. Collectively, our results further support evidence of protective functions for IFNγ and implicate BATF2 as a key suppressor of overactive immune signaling in astrocytes during neuroinflammation.

Graphical Abstract

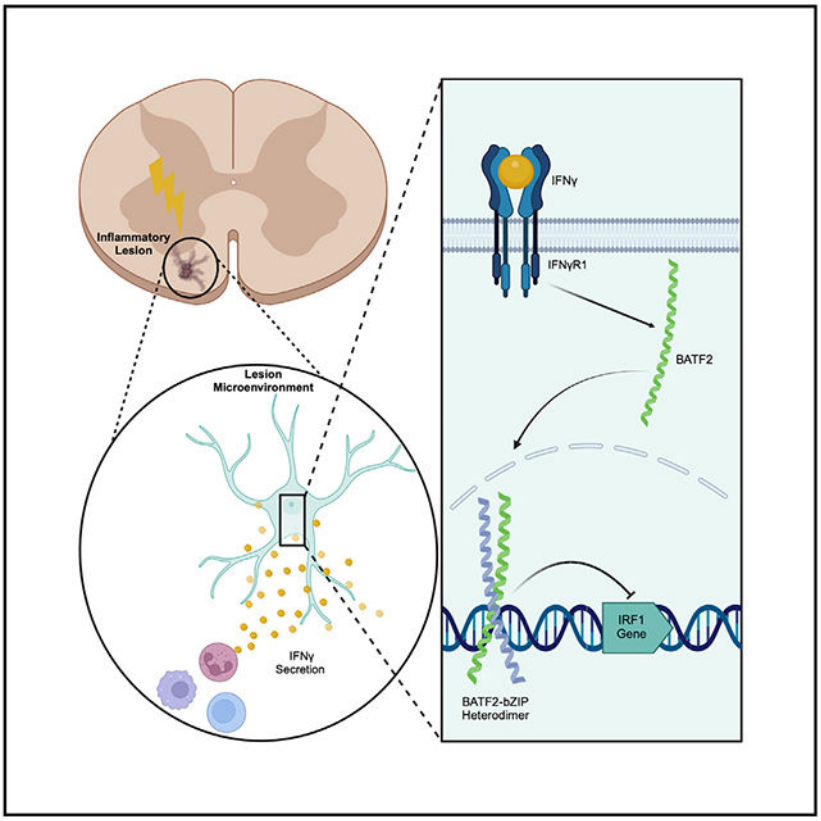

In brief

Tinkey et al. demonstrate that the upregulation of BATF2 downstream of IFNγ regulates the inflammatory potential of astrocytes during neuroinflammation. *In vivo* evidence suggests that BATF2 limits CNS autoimmunity and the expression of IFNγ-driven inflammatory mediators. These data suggest that BATF2 contributes to protective mechanisms in astrocytes during chronic neuroinflammation.

INTRODUCTION

Astrocytes are the most abundant glial cells in the central nervous system (CNS) and are essential for both homeostatic function and response to injury and disease. Assuming diverse phenotypes, morphologies, and functional properties, astrocytes are uniquely poised to respond to complex cues in the CNS microenvironment that result in both protective and pathogenic outcomes.[1] Widespread astrocyte reactivity is a common pathological hallmark across a variety of neuroinflammatory diseases, such as multiple sclerosis (MS), in which prolonged astrocyte activation contributes to early lesion formation and

sustained inflammation.[2,3] While changes in astrocytic function can be stimulated by a variety of factors, a major contributor, particularly in neuroinflammatory disorders like MS, includes cytokines, such as interferon (IFN)γ, that are highly pleiotropic in nature. Astrocyte exposure to IFNγ has previously been shown to contribute to sustained inflammation and neuronal damage through the initiation of cytokine production early in disease development.[3-5] However, IFNγ signaling in astrocytes has also been associated with protection from demyelination and clinical decline in progressive stages of immune-mediated neuroinflammation.[6-8] Further, we and others have recently shown additional protective roles for astrocytic IFNγ signaling, specifically in the spinal cord in an animal model of MS, experimental autoimmune encephalomyelitis (EAE).[9-12]

While several avenues of astrocytic IFNγ signaling have been described, the molecules responsible for directly regulating this protection are currently unknown. A variety of downstream effectors, namely transcription factors, play a major role in the regulation of gene expression and can be directly stimulated by IFNγ. Using RNA sequencing of primary human astrocytes treated with IFNγ, we identified the basic leucine zipper (bZIP) ATF-like transcription factor (*BATF*)2 as one of the most highly upregulated genes. BATF2 is a member of the bZIP family of transcription factors and was initially identified as an inhibitor of activator protein (AP)-1 function through direct interaction with c-JUN.[13] A pleiotropic immunomodulatory role for BATF2 has been demonstrated in peripheral models of inflammation in which BATF2 exerts both pro-inflammatory and protective functions. Specifically, BATF2 dimerization with c-JUN resulted in a reduction of interleukin (IL)-23 signaling during *Trypanosoma cruzi* infection[14] and attenuated colon inflammation by promoting the degradation of signal transducer and activator of transcription (STAT)1 in mice affected with colitis.[15] Conversely, BATF2 has also been shown to interact with other IFNγ-inducible transcription factors, including IFN regulatory factor (IRF)1, which is known to promote macrophage activation and enhance inflammation in several contexts.[16-18]

Due to its known activity in response to cytokine stimulation and extensive regulatory role in the periphery, BATF2 is a prime candidate for the modulation of neuroinflammatory events; however, the role of BATF2 in the CNS has not yet been described. In this study, we demonstrate that primary human astrocytes upregulate BATF2 in an IFNγ-specific manner and that IFNγ promotes the nuclear expression of BATF2, which may regulate AP-1 transcription sites. This nuclear BATF2 then suppresses overexpression of IRF1 and IRF1 target genes, such as caspase-1, that have been implicated as pro-inflammatory and deleterious during autoimmune demyelination.[19-23] Utilizing EAE as a model for neuroinflammation, we also show that *Batf2*$^{-/-}$ mice exhibit exacerbated EAE severity, characterized by an increase in both peripheral immune cell infiltration and demyelination compared to *Batf2*$^{+/+}$ controls. Further, *Batf2*$^{-/-}$ mice also exhibit increased astrocyte-specific expression of both IRF1 and caspase-1, suggesting an increased inflammatory phenotype driven, in part, by an enhanced IFN response *in vivo*. BATF2 was also found to be primarily expressed by astrocytes in MS lesions and colocalize with IRF1. Taken together, these data suggest that IFNγ-mediated BATF2 expression in astrocytes may directly facilitate a neuroprotective microenvironment downstream of IFNγ signaling during MS and EAE. These findings further enhance our current understanding

of immune-mediated CNS repair mechanisms driven by alternate astrocytic states during neuroinflammatory disease.

RESULTS

IFNγ enhances BATF2 expression in human astrocytes

We have previously identified protective mechanisms of IFNγ in astrocytes during chronic autoimmunity[9,24]; however, the specific intrinsic mechanisms responsible for regulating these pathways have not been fully elucidated. To investigate potential regulators of astrocytic IFNγ signaling, we performed RNA sequencing of primary human astrocytes (Figure S1A) treated with cytokines known to be present during a variety of neuroinflammatory events including IFNγ, tumor necrosis factor (TNF)-α, IL-1β, IL-17, and granulocyte-macrophage colony-stimulating factor (GM-CSF). Since the primary pathological target during EAE is the spinal cord and over 70% of patients with MS present with spinal cord lesions,[25,26] we focused our analysis on this CNS region. Principal-component analysis (PCA) revealed a heterogeneous response of spinal cord astrocytes to different cytokines, with IFNγ treatment having the greatest separation from media, followed by TNF-α and IL-1β, while IL-17 and GM-CSF remained the most similar to control-treated astrocytes (Figure 1A). To highlight genes specific to IFNγ, the top upregulated genes were compared to media-treated genes and plotted on a heatmap comparing expression patterns to TNF-α and IL-1β (Figure 1B). Genes exclusive to IFNγ treatment included *HLA-DMB*, *HLA-DQB1*, *HLA-DOA*, *INHBE*, *IL18BP*, and *BATF2* (Figure 1C). *HLA-DMB*, *HLA-DQB1*, and *HLA-DOA* transcribe proteins involved in major histocompatibility complex (MHC) class II antigen presentation,[27] while *INHBE* transcribes the preproprotein inhibin subunit βE, which is primarily expressed in the pancreas and liver and is a member of the transforming growth factor β superfamily.[28] Further, the *IL18BP* gene transcribes IL-18 binding protein that functions to inhibit IL-18 signaling.[29] Interestingly, of the genes identified as being IFNγ specific, *BATF2* was the only gene responsible for producing a transcription factor, and BATF2 had previously been shown to regulate inflammatory processes in the periphery.[14,16,17,30] To confirm the transcriptional regulation of *BATF2* by IFNγ, we treated primary human astrocytes over time and found that peak *BATF2* expression occurred at 12–24 h post-treatment (Figure 1D). Importantly, *BATF2* expression was specific to IFNγ compared to other inflammatory mediators and BATF family members (Figure 1E). While a dose titration using type I, II, and III IFNs revealed that the *BATF2* transcript was upregulated in astrocytes by both IFNγ and IFNβ, IFNγ was significantly more proficient at promoting *BATF2* expression (Figure S1B). Further, astrocyte BATF2 protein levels were elevated 24 h after IFNγ stimulation (Figures 1F and 1G). These data suggest that IFNγ signaling in astrocytes is sufficient to upregulate the transcription and protein expression of BATF2 in a specific manner.

IFNγ regulates BATF2 transcriptional activity

The function of BATF2 in the CNS and astrocytes has yet to be explored. To determine the chromatin occupancy of BATF2 at specific gene targets downstream of IFNγ, we treated primary human spinal cord astrocytes with IFNγ or a media control for 24 h and processed samples for chromatin immunoprecipitation (ChIP) sequencing, which

was performed and analyzed by Active Motif. Correlation coefficients of called peaks between treatments demonstrated high congruency between the media and IFNγ samples (Figure S2A), indicating high reproducibility among replicates. A relatively high correlation between the media and IFNγ samples was also found but was not unexpected, as BATF2 is known to be constitutively expressed, suggesting a potential overlap in transcriptional targets between media and IFNγ treatments. In order to tease out specific differences in peak metrics between the media and IFNγ samples, intervals of genomic regions with local enrichments in BATF2 tag numbers were grouped into merged peak regions. Notably, human astrocytes treated with IFNγ demonstrated an increased number of merged peak regions compared to media controls (Figure 2A). Specifically, 326 merged regions were found to be IFNγ specific, compared to 2 regions within media samples, and 97 regions were overlapped across all replicates of each treatment group (Figure S2B). Additionally, IFNγ-treated astrocytes also demonstrated a higher average peak tag number per merged region (Figure 2B), suggesting increased BATF2 chromatin accessibility and transcriptional activity with IFNγ stimulation. Peak enrichments at specific genomic loci were also identified and compared between media- and IFNγ-treated samples. Human astrocytes treated with IFNγ had an overall increase in BATF2 binding events throughout the genome as well as specific enrichments at both promoter regions and CpGI islands (Figure 2C). This suggests that there is increased recruitment of BATF2 to upstream and downstream transcriptional sites that have a direct impact on gene expression. Further, DNA motif analysis of media-stimulated astrocytes showed BATF2 binding at nuclear factor (NF)Y sites associated with CCAAT boxes (Figure 2D). NFY is a highly conserved heterotrimeric transcription factor necessary for the expression of genes involved in the cell cycle, DNA repair, and transcription initiation.[31-33] Conversely, following IFNγ treatment, we observed a significant increase in BATF2 binding at AP-1 sites (Figure 2E), suggesting that IFNγ-mediated BATF2 regulation of AP-1 may influence proliferation and/or critical inflammatory pathways in the CNS.[34-37] Taken together, these data suggest that IFNγ induces the transcriptional activity of BATF2 and shifts BATF2 function from modulating normal cellular processes to modulating those involved in neuroinflammation.

BATF2 suppresses IRF1 overexpression downstream of IFNγ in astrocytes

To identify specific pathways regulated by BATF2 downstream of IFNγ, we performed ingenuity pathway analysis (IPA) on annotated genes bound upstream or downstream by BATF2 in treated astrocytes. IPA identified several inflammatory pathways significantly associated with BATF2-bound regions, including the IFNγ and MS signaling pathways (Figure 3A). Additionally, regions associated with BATF2 binding were predicted to be activated by upstream regulators such as IFNγ and have both direct and indirect interactions with a variety of other immune function modulators (Figure 3B). This may suggest a potential role for BATF2 in several inflammatory mechanisms adjacent to IFNγ signaling. Further analysis of the IFNγ and MS pathways (Figures 3C and 3D) identified IRF1 as a common gene associated with increased BATF2 binding at upstream CpGI island regions in astrocytes stimulated with IFNγ compared to media controls (Figure 3E). To validate how the IRF1 signaling axis was regulated by BATF2, control or *Batf2*$^{-/-}$ murine astrocytes were stimulated with media or IFNγ for 48 h, and the levels of *Irf1* transcript, as well as IRF1 target genes, including *Psmb8*, *Casp1*, *Mhc1*, *Tap1*, and *Tap2*, were quantified. We

confirmed that there was no compensatory upregulation of other BATF family members and verified the deletion of the *Batf2* transcript as a control (Figure S3A). Notably, the loss of BATF2 resulted in increased expression of IRF1 as well as downstream IRF1 targets (Figures 3F-3K). These data suggest that BATF2 is necessary to govern IFNγ-inducible genes such as IRF1 and that deletion of BATF2 results in amplified IFNγ signaling in astrocytes.

Deletion of BATF2 exacerbates EAE

We and others have previously shown that dysregulated IFNγ signaling leads to exacerbation of EAE.[7-9,24] Moreover, with a focus on peripheral immune cells, other BATF family members have been studied in the context of EAE.[38,39] However, the impact of BATF2 on the CNS during neuroinflammation has yet to be described. Initially, we wanted to confirm that BATF2 was expressed in astrocytes *in vivo*. To demonstrate this, we injected TdTomato::*Aldh1l1*-Cre^{ERT2+} mice with tamoxifen to induce TdTomato expression in astrocytes. Following administration of tamoxifen, mice were immunized for EAE (Figure S4A). At peak disease, spinal cord tissue was harvested and processed for fluorescence-activated cell sorting (FACS). TdTomato$^+$ACSA2$^+$ astrocytes, CD4$^+$ T cells, and CD11b$^+$ myeloid cells were sorted and *Batf2* transcript expression was quantified in each population using qPCR. Notably, astrocytes were found to express *Batf2* at levels comparable to the myeloid compartment, while T cells showed little to no *Batf2* expression (Figures S4B-S4J).

Similarly, to validate that astrocytic BATF2 expression was dependent on IFNγ signaling *in vivo*, TdTomato::*Aldh1l1*-Cre^{ERT2+} *Ifngr1*$^{fl/fl}$ mice[9] and littermate controls were injected with tamoxifen to conditionally delete the IFNγ receptor on astrocytes. Mice were then immunized for EAE, and BATF2 expression was assessed. As expected, TdTomato::*Aldh1l1*-Cre^{ERT2+} *Ifngr1*$^{fl/fl}$ mice exhibited exacerbated EAE severity compared to littermate controls (Figure S5A). TdTomato$^+$ cells were confirmed as astrocytes via colocalization with SOX9 (Figures S5B-S5D). Importantly, there was a significant decrease in both total BATF2 expression and BATF2 colocalized with both SOX9$^+$ and TdTomato$^+$ astrocytes within lesions of *Aldh1l1*-Cre^{ERT2+} *Ifngr1*$^{fl/fl}$ mice compared to littermate controls (Figure S5E-S5K). Of note, the TdTomato$^+$ area was unchanged between genotypes (Figure S5L), indicating that deletion of the IFNγ receptor did not change the total number of astrocytes. Together, these results suggest that full BATF2 expression in astrocytes requires intact IFNγ signaling.

To further address how BATF2 directly modulates neuroinflammation, we induced EAE in *Batf2*$^{-/-}$ mice and controls. *Batf2*$^{-/-}$ mice were validated via qPCR (Figures S3A-S3C) and immunohistochemistry (Figures S3D-S3G) prior to use. Following EAE induction, *Batf2*$^{-/-}$ mice exhibited an exacerbated clinical disease course (Figures 4A and 4B), as well as increased demyelination, lesion size, and immune cell infiltration compared to littermate controls (Figures 4C-4I). To assess if *Batf2*$^{-/-}$ mice had dysregulated IFNγ signaling, we quantified IRF1 and caspase-1 protein levels in the ventral spinal cord white matter tracks and found that *Batf2*$^{-/-}$ mice had a significant increase in both IRF1 and caspase-1 expression within EAE lesions. Importantly, this increase was observed specifically in astrocytes compared to non-astrocytes, validating previous *in vitro* findings (Figures 4J-4U).

Taken together, these data suggest that BATF2 is protective during neuroinflammation and may act as a negative regulator of IFNγ-induced inflammatory pathways *in vivo* to limit immune-mediated CNS injury.

BATF2 is expressed in astrocytes within MS lesions

To determine if BATF2 may also have a role in MS, we first characterized its expression in chronic active white matter lesions. These lesions are one of the hallmarks of the chronic, progressive stage of disease in which IFNγ signaling is thought to confer protection.[6-9,24] Using postmortem MS tissue (Table 1), we identified chronic active lesions and normal-appearing white matter (NAWM) based on the presence or absence of myelin basic protein (MBP) and the classic myeloid cell rim using ionized calcium-binding adaptor molecule (IBA)1 labeling (Figure 5A). We then assessed the lesion rim, lesion core, and NAWM using immunofluorescence imaging of BATF2 and IRF1 and found that both were significantly upregulated in the lesion compared to NAWM. Interestingly, within the lesion, BATF2 and IRF1 were more highly expressed in the core compared to the lesion rim (Figures 5B-5E). Further colocalization analysis demonstrated that BATF2 and IRF1 expression within the core was more closely associated with $SOX9^+$ astrocytes than $IBA1^+$ myeloid cells (Figures 5F and 5G). SOX9 nuclear localization within MS lesions was confirmed via immunofluorescent imaging using DAPI as a counterstain (Figures S6A-S6E). Finally, we found that IRF1 tended to colocalize with BATF2 more readily in the lesion core compared to the rim (Figure 5H). These data demonstrate that both BATF2 and IRF1 are expressed in astrocytes in chronic active lesions and their co-expression may suggest that downstream of IFNγ signaling, BATF2 might regulate IRF1 function during MS to prevent excessive inflammation, particularly in the lesion core.

DISCUSSION

Growing evidence suggests that astrocytes may play a significant protective role in response to inflammatory stimuli during CNS disease. Notably, astrocytic reactivity in the form of scar-like barrier formation has been shown to limit parenchymal leukocyte infiltration during neuroinflammatory models such as EAE, and the ablation of reactive astrocytes exacerbates immune cell entry and clinical disease.[40] Further, the deletion of astrocyte-specific neuroprotective molecules, such as A20, which suppresses the activity of downstream inflammatory mediators like STAT1 and NF-κB, has led to more severe EAE and overactive immune signaling.[41] These data suggest that astrocytes are necessary to limit excessive inflammation in the CNS. Interestingly, pro-inflammatory cytokines, such as IFNγ, have been shown to drive specific facets of astrocyte neuroprotection, such as the upregulation of immune checkpoint inhibitors, as well as enhance resistance to damage induced by reactive oxygen species.[9,10] Moreover, IFNγ produced by natural killer cells in the meninges, enabled by the gut microbiome, has been shown to maintain a specific sub-population of astrocytes that express lysosomal-associated membrane protein 1 and TNF-related apoptosis-inducing ligand to limit neuroinflammation through the induction of apoptosis in T cells.[12] In this study, we extend these findings to reveal a novel transcriptional regulator of IFNγ-mediated protection in astrocytes. Our study demonstrates that the transcription factor BATF2 is upregulated in response to IFNγ stimulation by astrocytes and

prevents over-abundant transcription of IFN-specific genes such as *IRF1* and its downstream targets. Furthermore, loss of BATF2 led to exacerbated EAE with an increase in peripheral immune cell infiltration, demyelination, and expression of IRF1 and caspase-1 by astrocytes within lesions. Colocalized BATF2 and IRF1 expression in astrocytes was also found to occur within chronic active MS lesions, suggesting a similar protective mechanism in human neuroinflammatory disease.

To date, the vast majority of BATF2 literature has been focused on its role in the periphery in order to potentiate inflammatory responses in the context of infection. Of note, BATF2 has been shown to facilitate the expression of inflammatory genes such as *Tnf*, *Ccl5*, and *Nos2* in bone marrow-derived macrophages downstream of IFNγ and during *Mycobacterium tuberculosis* (Mtb) infection *in vitro*. This effect was thought to result from BATF2 dimerization with IRF1, suggesting that a pro-inflammatory BATF2-IRF1 signaling axis exists in macrophages.[16] Further *in vivo* studies of Mtb infection in *Batf2*-deficient mice demonstrated reduced inflammatory chemokine and cytokine responses in lung macrophages, leading to decreased pulmonary inflammation and increased survival, suggesting that a BATF2-associated inflammatory signature contributes to Mtb-associated mortality.[18] Contradictory to this evidence, during acute murine schistosomiasis infection, loss of BATF2 resulted in an exacerbated immune response, leading to increased TNF-α secretion by cells of the small intestine and enhanced T cell and dendritic cell activation.[18] A similar phenotype was observed in a murine model of colitis in which BATF2 deficiency increased CCL2 secretion through overactivation of STAT1 in intestinal epithelial cells.[15] Together, these previous studies suggest that BATF2 function is dependent on the context and nature of the immune response, as it has been shown to promote inflammation downstream of type 1 responses but is immunomodulatory during type 2 immunity in the periphery. Our data add complexity to BATF2 function as we demonstrate a protective role for BATF2 in astrocytes downstream of IFNγ, a classic type 1 neuroinflammatory response, in an animal model of MS, contradicting peripheral phenotypes. We also show that BATF2 suppresses overactive IRF1 signaling in astrocytes rather than the synergistic pro-inflammatory BATF2-IRF1 interaction seen in macrophages. These discrepancies suggest that cells of the CNS respond uniquely to inflammatory stimuli and that the pathological location and immune response type may also influence whether BATF2 functions in a deleterious or protective capacity. Further, these functional disparities could be driven by cell type, as astrocytes have been shown to respond differently to IFNα stimulation compared to myeloid cells such as microglia.[42] As such, it is possible that these distinctions extend to type II and III IFNs, as well as other cytokine families, and may point to fine-tuned specialization in CNS cell function that contributes to the divergent BATF2 response observed across cell types.

Within the context of neuroinflammatory disease, our study highlights the importance of BATF2 in the regulation of active IFN signaling during CNS autoimmunity, as we have shown that BATF2 negatively regulates critical inflammatory genes downstream of IFNγ in astrocytes. These genes include *Irf1* and *Casp1*, which are known to perpetuate inflammatory cascades that contribute to tissue damage during EAE.[19-23] Specifically, IRF1 and caspase-1 colocalize in astrocytes within demyelinating lesions, and mice lacking IRF1 failed to induce caspase-1 expression and were resistant to EAE. This observation may also

be facilitated by CNS resident cells, as bone marrow chimera experiments revealed that only *Irf1*$^{-/-}$ mice receiving wild-type bone marrow were protected from severe EAE compared to controls.[20] Further, expression of a dominant-negative form of IRF1 in oligodendrocytes ameliorated EAE and contributed to a reduced lesion load and parenchymal infiltration, confining immune cells largely to the perivascular space.[21] This suggests that IRF1 and subsequent activation of downstream genes may contribute to chemotaxis as well as the parenchymal invasion of peripheral immune cells during neuroinflammation. Our findings corroborate these studies, as we demonstrate that *Batf2*$^{-/-}$ mice express increased IRF1 and caspase-1 and have more extensive parenchymal infiltration during EAE compared to controls, suggesting that BATF2 suppression of IRF1 may work to limit CNS immune cell infiltration.

IRF1 single-nucleotide polymorphisms are also associated with progressive MS,[43] and IRF1 expression has been characterized within glial cells in chronic active MS lesions.[20] However, little is known about how IRF1 expression is regulated at the cellular level within the lesion microenvironment. Our study demonstrated that IRF1 and BATF2 expression was frequently colocalized in glial cells within chronic active lesions. Interestingly, this colocalization occurred most frequently in the lesion core within astrocytes, suggesting that BATF2 may be upregulated to suppress IRF1-induced inflammation in the quiescent lesion core. Cytokines, including IFNγ, are known inducers of astrocyte activation and may be released by activated myeloid cells within the lesion rim and contribute to scar formation.[44,45] While glial scarring is thought to inhibit remyelination, it is also essential for inflammatory confinement and protection of damaged axons.[46-49] Given the demonstrated protective capacity of astrocytic BATF2 downstream of IFNγ signaling and colocalization with inflammatory factors such as IRF1 in MS lesions, the specific upregulation of BATF2 within the lesion core may act as a facilitator of tissue sparing or repair.

Finally, loss of BATF2 has been linked to hyperactive IFN signaling and subsequent development of epilepsy and severe cognitive disability. Specifically, patients with a homozygous stop-gain mutation of *BATF2* presented with upregulated IFN-specific gene signatures in whole blood, resembling a type I IFN phenotype that is closely associated with interferonopathy.[50] Additionally, peripheral immune cells of patients with non-functional BATF2 were hyper-responsive to Toll-like receptor activation and overexpressed inflammatory cytokines, including IFNα, TNF, IL-6, and IL-23.[50] This may indicate that BATF2 has the ability to cross-regulate other inflammatory pathways in addition to those directly downstream of IFNs. Interestingly, IFNγ can suppress IL-1β signaling through a variety of mechanisms, including the inhibition of AP-1 and downstream mitogen-activated protein kinase pathways.[51-54] Astrocytic BATF2 may, therefore, be a key regulator of other neuroinflammatory signaling mechanisms, which may be applicable across many neurological disorders and warrants further investigation.

Limitations of the study

Our current study provides valuable insight into the role of BATF2 within astrocytes and neuroinflammatory disease; however, one notable limitation is the use of a global *Batf2*-deficient mouse to determine the astrocytic function of BATF2 during EAE. While we

validated astrocyte protein and transcript expression of BATF2 both *in vitro* and *in vivo*, as well as characterized the specific pro-inflammatory effects of BATF2 loss in astrocytes, consistent with previous literature, we did find that BATF2 was also expressed in the myeloid compartment. As such, future studies specifically deleting *Batf2* in myeloid cells and astrocytes will aid in further elucidating the cell-specific impact of BATF2 during EAE. Additionally, in this study, we demonstrate that BATF2 and IRF1 are co-expressed by astrocytes in MS lesions; however, the regulation of IRF1 by BATF2 in MS remains unknown. While we hypothesize that the core-specific upregulation of BATF2 may play a role in dampening inflammation, in part due to suppression of IRF1 overactivation, more direct evidence is required to fully clarify this pathway and its potential targeting for clinical translation.

STAR★METHODS

EXPERIMENTAL MODEL AND STUDY PARTICIPANT DETAILS

Animals—C57BL/6NJ and *Batf2*$^{-/-}$ mice (strain no. 031903) were obtained from The Jackson Laboratories. All mice were subjected to EAE induction at 9–10 weeks of age and were of mixed sex. All housing, breeding, and procedures were approved by the Institutional Animal Care and Use Committee at the Lerner Research Institute, Cleveland Clinic Foundation (Cleveland, OH) using protocol number 1862. All mice used were on a C57BL/6NJ background, were maintained on a 14/10h light/dark cycle and had *ad libitum* access to food and water. Mice (housed 2–5/cage) did not have any prior history of drug administration, surgery, or behavioral testing.

Primary human and murine astrocyte cultures—Primary human spinal cord astrocytes were obtained commercially from ScienCell Laboratories and grown according to provided protocols in complete ScienCell Astrocyte Medium. Briefly, astrocytes were isolated from the spinal cord and morphology was assessed by phase and relief contrast microscopy and GFAP positivity by immunofluorescence. Cell number, viability (≥70%), proliferative potential (≥15 pd), and negative screening for potential biological contaminants and mycoplasma was confirmed by ScienCell prior to cryopreservation. Following receipt, astrocytes were passaged and P3 cells were used for all studies and randomly allocated to treatment group. qPCR analysis for astrocyte purity was conducted prior to use in all experiments (Figure S1A).

Primary murine spinal cord astrocytes were harvested as previously described[55] with minor modifications. P2-P4 pups were euthanized and spinal cords harvested via hydro-ejection with PBS in ice-cold, serum free DMEM containing 1% penicillin/streptomycin. The spinal cords were then digested with gentle agitation for 15 min in 0.25% trypsin-EDTA. Trypsinization was stopped by adding DMEM media supplemented with 10% heat inactivated FBS and 1% penicillin/streptomycin. Cells were then treated with 50 μg/mL of DNase I for 3 min. Single cell suspensions were then made via trituration and cells were pelleted via centrifugation at 500x*g* for 5 min. Cells were resuspended in 10% DMEM and plated onto fibronectin-coated plates. Cells received a complete media change every other

day until reaching 80% confluency. Astrocytes were mechanically separated from microglia and oligodendrocyte progenitor cells via orbital shaking.

Postmortem human MS tissue—Periventricular white matter from MS patients (Table 1) was collected according to the established rapid autopsy protocol approved by the Cleveland Clinic Institutional Review Board. A total of 6 MS patients with secondary progressive (SP) MS and primary progressive (PP) MS were used for analysis. Patients consisted of 3 males and 3 females with ages ranging from 27 to 67 years. MS patient tissue was prepared in 1cm thick slices using a guided box and was fixed in 4% paraformaldehyde (PFA) followed by sectioning for morphological and immunohistochemical analysis. Chronic active lesions were identified using immunofluorescent analysis (Figure 5A) and target proteins were compared within each individual lesion per patient.

METHOD DETAILS

EAE induction—Mice of mixed sex were induced for EAE at 9–10 weeks of age. C57BL/6NJ and *Batf2*$^{-/-}$ mice were obtained commercially from The Jackson Laboratories and housed under specific pathogen-free conditions. *Batf2*$^{+/-}$ mice were bred together to obtain littermate controls. C57BL/6NJ mice were bred together and used as controls. On day 0, mice were immunized s.c. with 100μg MOG_{35-55} emulsified in complete Freund's adjuvant containing 400mg of heat killed Mycobacterium tuberculosis H37Ra using a standard emulsion (Hooke Laboratories). Pertussis toxin (100ng) (Hooke Laboratories) was injected i.p. on the day of immunization and two days later. Mice were monitored daily for clinical signs of disease as follows: 0, no observable signs; 1, limp tail; 2, limp tail and ataxia; 2.5, limp tail and knuckling of at least one limb; 3, paralysis of one limb; 3.5, partial paralysis of one limb and complete paralysis of the other; 4, complete hindlimb paralysis; 4.5, moribund; 5, death. Animals that did not develop clinical signs of EAE were excluded from the study. On day 25, mice were euthanized for histological studies via transcardial perfusion with PBS and 4% PFA. Mice were dissected to preserve spinal cord tissue integrity followed by fixation in 4% PFA overnight. Tissue was then transferred to a 30% sucrose solution for cryopreservation and spinal cords were frozen in O.C.T. Compound (Fisher Healthcare). Frozen, transverse sections (10mm) were slide mounted and stored at −80°C until immunofluorescent labeling.

Immunofluorescent labeling—Tissue sections were blocked with 10% goat serum (Sigma) and 0.1% Triton X-100 for 1h at room temperature and then incubated with anti-MBP (Abcam), anti-GFAP (Invitrogen), CD45 PerCP-Cy5.5 (Biolegend), and anti-Caspase1 (Abclonal) primary antibodies overnight at 4°C. Tissue sections labeled with anti-IRF1 (Cell Signaling) and anti-SOX9 (Novus) were subjected to antigen retrieval by boiling the tissue in a decloaking chamber for 5 min at 95°C in a 10mM Tris and 1mM EDTA buffer prior to blocking and then incubated in primary antibody as previously described. Secondary antibodies conjugated to Alexa Fluor 488, Alex Fluor 555, and Alexa Fluor 647 (Invitrogen) were applied for 1h at room temperature as appropriate. Nuclei were counterstained with DAPI (Thermofisher) diluted in PBS. Sections were imaged using the 20x objective of a confocal microscope LSM 800 (Carl Zeiss). Representative images shown are illustrative of 3–6 images taken across two or more tissue sections at least 100μm apart per individual

mouse. The mean positive area and Mander's coefficient of colocalization were determined by setting thresholds using appropriate controls and quantified using ImageJ software (NIH). The mean positive area and Mander's coefficient per image were averaged across individual animals to represent data points depicted. Lesion area was determined by tracing the area of mononuclear cell infiltration, using DAPI and CD45 staining, into the parenchyma using ImageJ software (NIH).

Free floating sections of human periventricular white matter were subjected to antigen retrieval by boiling the tissue briefly in 10μM citrate buffer. Sections were blocked with 5% donkey serum and 0.03% Triton X-100 (Sigma Aldrich) for 1h at room temperature. Demyelinated lesions were identified and characterized using immunostaining for MBP (Abcam) and IBA1 (Wako) as previously described.[9,24] Subsequent sections were exposed to antibodies specific for human BATF2 (Santa Cruz), IRF1 (Proteintech), Sox9 (R&D Systems), ALDH1L1 (Cell Signaling), and/or IBA1 (SPICA Dye 594-conjugated; Wako) for 4–5 days at 4°C. Sections were then washed with PBS-Triton-X-100, and secondary antibodies conjugated to Alexa Fluor 405, 488, and 647 (Thermofisher) were applied for 1h at room temperature as appropriate. Sections were then treated with 0.3% Sudan black in 70% ethanol for 3 min, imaged using the 10x, 20x, 40x, and 63x objectives of a confocal microscope LSM 800 (Carl Zeiss). Resulting images were analyzed using ImageJ and Fiji software (NIH). The mean positive area and Mander's coefficient of colocalization were determined by setting thresholds using appropriate controls. Representative images shown are illustrative of 3–6 images per patient across one or more chronic active lesions. The mean positive area and Mander's coefficient of colocalization were determined by setting thresholds using appropriate controls and quantified using ImageJ software (NIH). The mean positive area and Mander's coefficient per image were averaged across each patient to represent data points depicted. Area and colocalization analyses within the lesion rim and core were determined by setting defined regions of interest using $IBA1^+$ area to define the lesion rim and lesion core for each patient. Three-dimensional reconstructions were generated using Imaris software.

RNA sequencing—Total RNA was collected from human primary spinal cord astrocytes (ScienCell) treated with recombinant human IFNγ, TNFα, IL-1β, IL-17, GMCSF, or media (Peprotech) for 24h using an RNeasy Mini Kit (Qiagen) according to the manufacturer's instructions and quantified using a NanoDrop One spectrophotometer (Thermofisher). RNA was then sequenced at the Cleveland Clinic Lerner Research Institute Genomics Core using an established pipeline.[56,57] Sequencing reads were generated from the Illumina platform and assessed for quality and trimmed for adapter sequences using TrimGalore! v0.4.2 (Babraham Bioinformatics), a wrapper script for FastQC and cutadapt. Reads that passed quality control were then aligned to the human reference genome (hg38) using the STAR aligner v2.5.3. The alignment for the sequences were guided using the GENCODE annotation for hg38. The aligned reads were analyzed for differential expression using Cufflinks v2.2.1, a RNASeq analysis package which reports the fragments per kilobase of exon per million fragments mapped (FPKM) for each gene. Differential analysis report was generated using the cuffdiff command performed in a pairwise manner for each group. Differential genes were identified using a significance cutoff of q-value <0.05. The

genes were then subjected to gene set enrichment analysis (GenePattern, Broad Institute) to determine any relevant processes that may be differentially overrepresented for the conditions tested.

Quantitative PCR (qPCR)—Total RNA was collected from human or murine primary spinal cord astrocytes following media or cytokine treatment using an RNeasy Mini Kit (Qiagen) according to the manufacturer's instructions and measured with a NanoDrop One spectrophotometer (Thermofisher). Total RNA was then normalized, treated with DNase I (Thermofisher), and reversed transcribed to cDNA using a TaqMan Reverse Transcription kit (Applied Biosciences). Prepared cDNA was then used as a template for qPCR using a QuantStudio 6 Real-Time PCR system (Thermofisher). Relative gene expression was quantified after normalizing to *GAPDH* expression. Primer sequences used are listed in the key resources table.[58]

Chromatin immunoprecipitation (ChIP) sequencing and pathway analysis—Primary human astrocytes were stimulated with media or 10 ng/mL IFNγ for 24h and fixed for 15 min in 1/10 volume Formaldehyde solution (11% Formaldehyde, 0.1M NaCl, 1mM EDTA pH 8.0, 50mM HEPES pH 7.9 in milliQ H_2O) at room temperature. Fixation was stopped by adding 1/20 volume glycine solution (2.5M in milliQ H_2O) for 5 min at room temperature. Cells were then scraped, transferred into 50mL conical tubes, and kept on ice. Tubes were centrifuged at 800x*g* at 4°C for 10 min. Pelleted cells were then resuspended in 10mL of chilled PBS-Igepal solution (0.5% Igepal in 1X PBS). Cells were repelleted as before and washed twice more with PBS-Igepal, adding 100uL of PMSF (1mM in ethanol) after the second wash to each sample. Pellets were then snap frozen on dry ice. Further processing for ChIP sequencing and analysis, including chromatin extraction, fragmentation, antibody precipitation, and library preparation was performed commercially by Active Motif Services using a validated antibody to BATF2 (Proteintech). Sequence libraries were generated using the standardized steps of enzymatic end polishing, dA-addition, and adaptor ligation. Following PCR amplification, the resulting libraries were quantified, sequenced, and quality filtered using the Illumina platform (75 nucleotide reads, single end). Reads were then aligned to the human genome (hg38) using the BWA algorithm. Duplicated reads were removed and uniquely mapped reads (≥25 mapping quality) that aligned with no more than 2 mismatches were used for downstream analysis. MACS software[59] (v 2.1.0) was used to call unique peaks relative to the pooled input with cutoffs of $1e^{-7}$ for narrow peaks and $1e^{-1}$ for broad peaks. Peaks were then filtered by removing false ChIP Seq peaks as defined by the ENCODE blacklist. Known motifs were identified using the findMotifsGenome program of the HOMER package[a] using default parameters and input sequences comprising +/− 100 bp from the center of the top 2500 peaks. Resulting signal maps were stored in bigWig files and also analyzed by Active Motif using proprietary analysis software. Excel files containing peak metrics, peak location, and gene information were generated. The resulting gene set associated with BATF2 chromatin binding was analyzed using IPA software (Ingenuity System Inc.) to examine canonical pathways regulated by BATF2 in media- and IFNγ-treated samples.

Lysate preparation and western blotting—Primary human spinal cord astrocytes were treated with media or 10 ng/mL IFNγ for 24h. Cells were trypsonized with 0.05% Trypsin EDTA and homogenized in RIPA lysis buffer (50mM Tris-HCl pH = 7.4, 150mM NaCl, 1mM EDTA, 1% Triton X-100, and 1:100 proteinase/phosphatase inhibitor). Samples were briefly triturated, vortexed for 3s, and incubated on ice for 30 min. For complete lysis, samples were frozen on dry ice for 3 min and thawed in wet ice for 15 min. A total of 3 freeze-thaw cycles were conducted. Samples were then centrifuged at 10,000x*g* for 30 min and supernatants were collected for immunoblotting. Protein levels were quantified using a Pierce BCA kit (Thermofisher) and normalized. 2x Laemmli sample buffer and b-Mercaptoethanol were added to normalized samples. 20μg of total protein lysate was resolved on Novex WedgeWell 4–20% Tris-Glycine gels and transferred to nitrocellulose membranes. The membranes were blocked with 5% low-fat powdered milk in Tris-buffered saline, 0.1% Tween 20 (TBST) for 1h at room temperature and incubated overnight at 4°C with primary antibody. Membranes were blotted with anti-BATF2 (Thermofisher) and anti-b-actin (ThermoFisher) antibodies. The following day, membranes were washed with TBST 3 times and incubated with HRP conjugated antibodies for 1h at room temperature. Membranes were then washed with TBST 3 times and imaged using the ChemiDoc MP imaging system (Bio-Rad) after activation with ECL substrate (Bio-Rad).

QUANTIFICATION AND STATISTICAL ANALYSIS

Statistical analysis—Data and statistical analysis were performed using Prism 10.1.2 (Graphpad). Significance criteria includes: ns (not significant), $p > 0.05$, $*p < 0.05$, $**p < 0.01$, $***p < 0.001$, and $****p < 0.0001$. Differences in means between greater than 2 groups were analyzed using a one-way ANOVA (with Tukey's post hoc correction for multiple comparisons). For mixed groups, a two-way ANOVA (with Tukey's post hoc correction for multiple comparisons) was used. EAE data were analyzed using the nonparametric Mann-Whitney *U* test. Graph bars indicate mean and error bars indicate standard error (SEM). For *in vivo* experiments, each *n* is representative of individual animals. For *in vitro* experiments, each *n* is representative of a separate, independent experiment. The *n* value for all experiments can be found in the provided Figure Legends.

Supplementary Material

Refer to Web version on PubMed Central for supplementary material.

ACKNOWLEDGMENTS

We thank Kaitlin Kaiser for her assistance with mouse colony management, husbandry, and genotyping and her contributions to the graphical abstract design. We also thank Dr. Bruce Trapp and Dr. Ranjan Dutta for sourcing human MS tissue, Orion Brock for insightful discussion, and Dr. Benjamin Shaw and Nancy A. Rebert for technical assistance with FACS processing. This work was supported by National Institute of Neurological Disorders and Stroke (NINDS) R01 NS119178 (awarded to J.L.W.) and R35 NS097303 (awarded to Bruce D. Trapp) and National MS Society RFA-2203-39228 (awarded to J.L.W.).

REFERENCES

1. Escartin C, Galea E, Lakatos A, O'Callaghan JP, Petzold GC, Serrano-Pozo A, Steinhäuser C, Volterra A, Carmignoto G, Agarwal A, et al. (2021). Reactive astrocyte nomenclature,

definitions, and future directions. Nat. Neurosci 24, 312–325. 10.1038/s41593-020-00783-4. [PubMed: 33589835]

2. Brosnan CF, and Raine CS (2013). The astrocyte in multiple sclerosis revisited. Glia 61, 453–465. 10.1002/glia.22443. [PubMed: 23322421]
3. Olsson T. (1992). Cytokines in neuroinflammatory disease: role of myelin autoreactive T cell production of interferon-gamma. J. Neuroimmunol 40, 211–218. 10.1016/0165-5728(92)90135-8. [PubMed: 1430152]
4. Fletcher JM, Lalor SJ, Sweeney CM, Tubridy N, and Mills KHG (2010). T cells in multiple sclerosis and experimental autoimmune encephalomyelitis. Clin. Exp. Immunol 162, 1–11. 10.1111/j.1365-2249.2010.04143.x. [PubMed: 20682002]
5. Hashioka S, McGeer EG, Miyaoka T, Wake R, Horiguchi J, and McGeer PL (2015). Interferon-γ-induced neurotoxicity of human astrocytes. CNS Neurol. Disord.: Drug Targets 14, 251–256. 10.2174/1871527314666150217122305. [PubMed: 25687700]
6. Sun L, Li Y, Jia X, Wang Q, Li Y, Hu M, Tian L, Yang J, Xing W, Zhang W, et al. (2017). Neuroprotection by IFN-γ via astrocyte-secreted IL-6 in acute neuroinflammation. Oncotarget 8, 40065–40078. 10.18632/oncotarget.16990. [PubMed: 28454116]
7. Hindinger C, Bergmann CC, Hinton DR, Phares TW, Parra GI, Hussain S, Savarin C, Atkinson RD, and Stohlman SA (2012). IFN-γ signaling to astrocytes protects from autoimmune mediated neurological disability. PLoS One 7, e42088. 10.1371/journal.pone.0042088. [PubMed: 22848713]
8. Savarin C, Hinton DR, Valentin-Torres A, Chen Z, Trapp BD, Bergmann CC, and Stohlman SA (2015). Astrocyte response to IFN-γ limits IL-6-mediated microglia activation and progressive autoimmune encephalomyelitis. J. Neuroinflammation 12, 79. 10.1186/s12974-015-0293-9. [PubMed: 25896970]
9. Smith BC, Tinkey RA, Brock OD, Mariam A, Habean ML, Dutta R, and Williams JL (2023). Astrocyte interferon-gamma signaling dampens inflammation during chronic central nervous system autoimmunity via PD-L1. J. Neuroinflammation 20, 234. 10.1186/s12974-023-02917-4. [PubMed: 37828609]
10. Smith BC, Sinyuk M, Jenkins JE, Psenicka MW, and Williams JL (2020). The impact of regional astrocyte interferon-gamma signaling during chronic autoimmunity: a novel role for the immunoproteasome. J. Neuroinflammation 17, 184. 10.1186/s12974-020-01861-x. [PubMed: 32532298]
11. Linnerbauer M, Beyer T, Nirschl L, Farrenkopf D, Lößlein L, Vandrey O, Peter A, Tsaktanis T, Kebir H, Laplaud D, et al. (2023). PD-L1 positive astrocytes attenuate inflammatory functions of PD-1 positive microglia in models of autoimmune neuroinflammation. Nat. Commun 14, 5555. 10.1038/s41467-023-40982-8. [PubMed: 37689786]
12. Sanmarco LM, Wheeler MA, Gutierrez-Vazquez C, Polonio CM, Linnerbauer M, Pinho-Ribeiro FA, Li Z, Giovannoni F, Batterman KV, Scalisi G, et al. (2021). Gut-licensed IFNgamma(+) NK cells drive LAMP1(+)TRAIL(+) anti-inflammatory astrocytes. Nature 590, 473–479. 10.1038/s41586-020-03116-4. [PubMed: 33408417]
13. Su ZZ, Lee SG, Emdad L, Lebdeva IV, Gupta P, Valerie K, Sarkar D, and Fisher PB (2008). Cloning and characterization of SARI (suppressor of AP-1, regulated by IFN). Proc. Natl. Acad. Sci. USA 105, 20906–20911. 10.1073/pnas.0807975106. [PubMed: 19074269]
14. Kitada S, Kayama H, Okuzaki D, Koga R, Kobayashi M, Arima Y, Kumanogoh A, Murakami M, Ikawa M, and Takeda K. (2017). BATF2 inhibits immunopathological Th17 responses by suppressing Il23a expression during Trypanosoma cruzi infection. J. Exp. Med 214, 1313–1331. 10.1084/jem.20161076. [PubMed: 28356392]
15. Dai L, Liu Y, Cheng L, Wang H, Lin Y, Shi G, Dong Z, Li J, Fan P, Wang Q, et al. (2019). SARI attenuates colon inflammation by promoting STAT1 degradation in intestinal epithelial cells. Mucosal Immunol. 12, 1130–1140. 10.1038/s41385-019-0178-9. [PubMed: 31182817]
16. Roy S, Guler R, Parihar SP, Schmeier S, Kaczkowski B, Nishimura H, Shin JW, Negishi Y, Ozturk M, Hurdayal R, et al. (2015). Batf2/Irf1 induces inflammatory responses in classically activated macrophages, lipopolysaccharides, and mycobacterial infection. J. Immunol 194, 6035–6044. 10.4049/jimmunol.1402521. [PubMed: 25957166]

17. van der Geest R, Penãloza HF, Xiong Z, Gonzalez-Ferrer S, An X, Li H, Fan H, Tabary M, Nouraie SM, Zhao Y, et al. (2023). BATF2 enhances proinflammatory cytokine responses in macrophages and improves early host defense against pulmonary Klebsiella pneumoniae infection. Am. J. Physiol. Lung Cell. Mol. Physiol 325, L604–L616. 10.1152/ajplung.00441.2022. [PubMed: 37724373]

18. Guler R, Mpotje T, Ozturk M, Nono JK, Parihar SP, Chia JE, Abdel Aziz N, Hlaka L, Kumar S, Roy S, et al. (2019). Batf2 differentially regulates tissue immunopathology in Type 1 and Type 2 diseases. Mucosal Immunol. 12, 390–402. 10.1038/s41385-018-0108-2. [PubMed: 30542107]

19. Furlan R, Martino G, Galbiati F, Poliani PL, Smiroldo S, Bergami A, Desina G, Comi G, Flavell R, Su MS, and Adorini L. (1999). Caspase-1 regulates the inflammatory process leading to autoimmune demyelination. J. Immunol 163, 2403–2409. [PubMed: 10452974]

20. Ren Z, Wang Y, Liebenson D, Liggett T, Goswami R, Stefoski D, and Balabanov R. (2011). IRF-1 signaling in central nervous system glial cells regulates inflammatory demyelination. J. Neuroimmunol 233, 147–159. 10.1016/j.jneuroim.2011.01.001. [PubMed: 21257209]

21. Ren Z, Wang Y, Tao D, Liebenson D, Liggett T, Goswami R, Clarke R, Stefoski D, and Balabanov R. (2011). Overexpression of the dominant-negative form of interferon regulatory factor 1 in oligodendrocytes protects against experimental autoimmune encephalomyelitis. J. Neurosci 31, 8329–8341. 10.1523/jneurosci.1028-11.2011. [PubMed: 21653838]

22. Buch T, Uthoff-Hachenberg C, and Waisman A. (2003). Protection from autoimmune brain inflammation in mice lacking IFN-regulatory factor-1 is associated with Th2-type cytokines. Int. Immunol 15, 855–859. 10.1093/intimm/dxg086. [PubMed: 12807824]

23. Tada Y, Ho A, Matsuyama T, and Mak TW (1997). Reduced incidence and severity of antigen-induced autoimmune diseases in mice lacking interferon regulatory factor-1. J. Exp. Med 185, 231–238. 10.1084/jem.185.2.231. [PubMed: 9016872]

24. Smith BC, Sinyuk M, Jenkins JE, Psenicka MW, and Williams JL (2020). The impact of regional astrocyte interferon-γ signaling during chronic autoimmunity: a novel role for the immunoproteasome. J. Neuroinflammation 17, 184. 10.1186/s12974-020-01861-x. [PubMed: 32532298]

25. Lycklama G, Thompson A, Filippi M, Miller D, Polman C, Fazekas F, and Barkhof F. (2003). Spinal-cord MRI in multiple sclerosis. Lancet Neurol. 2, 555–562. 10.1016/s1474-4422(03)00504-0. [PubMed: 12941578]

26. Nijeholt GJ, van Walderveen MA, Castelijns JA, van Waesberghe JH, Polman C, Scheltens P, Rosier PF, Jongen PJ, and Barkhof F. (1998). Brain and spinal cord abnormalities in multiple sclerosis. Correlation between MRI parameters, clinical subtypes and symptoms. Brain 121, 687–697. 10.1093/brain/121.4.687. [PubMed: 9577394]

27. Handunnetthi L, Ramagopalan SV, Ebers GC, and Knight JC (2010). Regulation of major histocompatibility complex class II gene expression, genetic variation and disease. Gene Immun. 11, 99–112. 10.1038/gene.2009.83.

28. Sugiyama M, Kikuchi A, Misu H, Igawa H, Ashihara M, Kushima Y, Honda K, Suzuki Y, Kawabe Y, Kaneko S, and Takamura T. (2018). Inhibin βE (INHBE) is a possible insulin resistance-associated hepatokine identified by comprehensive gene expression analysis in human liver biopsy samples. PLoS One 13, e0194798. 10.1371/journal.pone.0194798. [PubMed: 29596463]

29. Dinarello CA, Novick D, Kim S, and Kaplanski G. (2013). Interleukin-18 and IL-18 binding protein. Front. Immunol 4, 289. 10.3389/fimmu.2013.00289. [PubMed: 24115947]

30. Kayama H, Tani H, Kitada S, Opasawatchai A, Okumura R, Motooka D, Nakamura S, and Takeda K. (2019). BATF2 prevents T-cell-mediated intestinal inflammation through regulation of the IL-23/IL-17 pathway. Int. Immunol 31, 371–383. 10.1093/intimm/dxz014. [PubMed: 30753547]

31. Oldfield AJ, Yang P, Conway AE, Cinghu S, Freudenberg JM, Yell-aboina S, and Jothi R. (2014). Histone-fold domain protein NF-Y promotes chromatin accessibility for cell type-specific master transcription factors. Mol. Cell 55, 708–722. 10.1016/j.molcel.2014.07.005. [PubMed: 25132174]

32. Oldfield AJ, Henriques T, Kumar D, Burkholder AB, Cinghu S, Paulet D, Bennett BD, Yang P, Scruggs BS, Lavender CA, et al. (2019). NF-Y controls fidelity of transcription initiation at gene promoters through maintenance of the nucleosome-depleted region. Nat. Commun 10, 3072. 10.1038/s41467-019-10905-7. [PubMed: 31296853]

33. Fleming JD, Pavesi G, Benatti P, Imbriano C, Mantovani R, and Struhl K. (2013). NF-Y coassociates with FOS at promoters, enhancers, repetitive elements, and inactive chromatin regions, and is stereo-positioned with growth-controlling transcription factors. Genome Res. 23, 1195–1209. 10.1101/gr.148080.112. [PubMed: 23595228]
34. Wei CJ, Li YL, Zhu ZL, Jia DM, Fan ML, Li T, Wang XJ, Li ZG, and Ma HS (2019). Inhibition of activator protein 1 attenuates neuroinflammation and brain injury after experimental intracerebral hemorrhage. CNS Neurosci. Ther 25, 1182–1188. 10.1111/cns.13206. [PubMed: 31392841]
35. Yamazaki S, Tanaka Y, Araki H, Kohda A, Sanematsu F, Arasaki T, Duan X, Miura F, Katagiri T, Shindo R, et al. (2017). The AP-1 transcription factor JunB is required for Th17 cell differentiation. Sci. Rep 7, 17402. 10.1038/s41598-017-17597-3. [PubMed: 29234109]
36. Bagnoud M, Briner M, Remlinger J, Meli I, Schuetz S, Pistor M, Salmen A, Chan A, and Hoepner R. (2020). c-Jun N-Terminal Kinase as a Therapeutic Target in Experimental Autoimmune Encephalomyelitis. Cells 9, 2154. 10.3390/cells9102154. [PubMed: 32977663]
37. Groves A, Kihara Y, Jonnalagadda D, Rivera R, Kennedy G, Mayford M, and Chun J. (2018). A Functionally Defined In Vivo Astrocyte Population Identified by c-Fos Activation in a Mouse Model of Multiple Sclerosis Modulated by S1P Signaling: Immediate-Early Astrocytes (ieAstrocytes). eNeuro 5. 10.1523/eneuro.0239-18.2018.
38. Schraml BU, Hildner K, Ise W, Lee WL, Smith WAE, Solomon B, Sahota G, Sim J, Mukasa R, Cemerski S, et al. (2009). The AP-1 transcription factor Batf controls T(H)17 differentiation. Nature 460, 405–409. 10.1038/nature08114. [PubMed: 19578362]
39. Karwacz K, Miraldi ER, Pokrovskii M, Madi A, Yosef N, Wortman I, Chen X, Watters A, Carriero N, Awasthi A, et al. (2017). Critical role of IRF1 and BATF in forming chromatin landscape during type 1 regulatory cell differentiation. Nat. Immunol 18, 412–421. 10.1038/ni.3683. [PubMed: 28166218]
40. Voskuhl RR, Peterson RS, Song B, Ao Y, Morales LBJ, Tiwari-Woodruff S, and Sofroniew MV (2009). Reactive astrocytes form scar-like perivascular barriers to leukocytes during adaptive immune inflammation of the CNS. J. Neurosci 29, 11511–11522. 10.1523/jneurosci.1514-09.2009. [PubMed: 19759299]
41. Wang X, Deckert M, Xuan NT, Nishanth G, Just S, Waisman A, Naumann M, and Schlüter D. (2013). Astrocytic A20 ameliorates experimental autoimmune encephalomyelitis by inhibiting NF-κB- and STAT1-dependent chemokine production in astrocytes. Acta Neuropathol. 126, 711–724. 10.1007/s00401-013-1183-9. [PubMed: 24077734]
42. Li W, Viengkhou B, Denyer G, West PK, Campbell IL, and Hofer MJ (2018). Microglia have a more extensive and divergent response to interferon-α compared with astrocytes. Glia 66, 2058–2078. 10.1002/glia.23460. [PubMed: 30051922]
43. Fortunato G, Calcagno G, Bresciamorra V, Salvatore E, Filla A, Capone S, Liguori R, Borelli S, Gentile I, Borrelli F, et al. (2008). Multiple sclerosis and hepatitis C virus infection are associated with single nucleotide polymorphisms in interferon pathway genes. J. Interferon Cytokine Res 28, 141–152. 10.1089/jir.2007.0049. [PubMed: 18338947]
44. Liddelow SA, Guttenplan KA, Clarke LE, Bennett FC, Bohlen CJ, Schirmer L, Bennett ML, Münch AE, Chung WS, Peterson TC, et al. (2017). Neurotoxic reactive astrocytes are induced by activated microglia. Nature 541, 481–487. 10.1038/nature21029. [PubMed: 28099414]
45. Wang H, Song G, Chuang H, Chiu C, Abdelmaksoud A, Ye Y, and Zhao L. (2018). Portrait of glial scar in neurological diseases. Int. J. Immunopathol. Pharmacol 31, 2058738418801406. 10.1177/2058738418801406. [PubMed: 30309271]
46. Bush TG, Puvanachandra N, Horner CH, Polito A, Ostenfeld T, Svendsen CN, Mucke L, Johnson MH, and Sofroniew MV (1999). Leukocyte infiltration, neuronal degeneration, and neurite outgrowth after ablation of scar-forming, reactive astrocytes in adult transgenic mice. Neuron 23, 297–308. 10.1016/s0896-6273(00)80781-3. [PubMed: 10399936]
47. Faulkner JR, Herrmann JE, Woo MJ, Tansey KE, Doan NB, and Sofroniew MV (2004). Reactive astrocytes protect tissue and preserve function after spinal cord injury. J. Neurosci 24, 2143–2155. 10.1523/jneurosci.3547-03.2004. [PubMed: 14999065]
48. Toft-Hansen H, Füchtbauer L, and Owens T. (2011). Inhibition of reactive astrocytosis in established experimental autoimmune encephalomyelitis favors infiltration by myeloid cells over

T cells and enhances severity of disease. Glia 59, 166–176. 10.1002/glia.21088. [PubMed: 21046558]

49. Liu Z, Li Y, Cui Y, Roberts C, Lu M, Wilhelmsson U, Pekny M, and Chopp M. (2014). Beneficial effects of gfap/vimentin reactive astrocytes for axonal remodeling and motor behavioral recovery in mice after stroke. Glia 62, 2022–2033. 10.1002/glia.22723. [PubMed: 25043249]
50. Zsurka G, Appel MLT, Nastaly M, Hallmann K, Hansen N, Nass D, Baumgartner T, Surges R, Hartmann G, Bartok E, and Kunz WS (2023). Loss of the Immunomodulatory Transcription Factor BATF2 in Humans Is Associated with a Neurological Phenotype. Cells 12, 227. 10.3390/cells12020227. [PubMed: 36672163]
51. Ho HH, Antoniv TT, Ji JD, and Ivashkiv LB (2008). Lipopolysaccha-ride-induced expression of matrix metalloproteinases in human monocytes is suppressed by IFN-gamma via superinduction of ATF-3 and suppression of AP-1. J. Immunol 181, 5089–5097. 10.4049/jimmunol.181.7.5089. [PubMed: 18802113]
52. Hu X, Paik PK, Chen J, Yarilina A, Kockeritz L, Lu TT, Woodgett JR, and Ivashkiv LB (2006). IFN-gamma suppresses IL-10 production and synergizes with TLR2 by regulating GSK3 and CREB/AP-1 proteins. Immunity 24, 563–574. 10.1016/j.immuni.2006.02.014. [PubMed: 16713974]
53. Radzioch D, and Varesio L. (1991). c-fos mRNA expression in macrophages is downregulated by interferon-gamma at the posttranscriptional level. Mol. Cell Biol 11, 2718–2722. 10.1128/mcb.11.5.2718-2722.1991. [PubMed: 1901945]
54. Hu X, Chen J, Wang L, and Ivashkiv LB (2007). Crosstalk among Jak-STAT, Toll-like receptor, and ITAM-dependent pathways in macrophage activation. J. Leukoc. Biol 82, 237–243. 10.1189/jlb.1206763. [PubMed: 17502339]
55. Sinyuk M, and Williams JL (2020). Dissection and Isolation of Murine Glia from Multiple Central Nervous System Regions. J. Vis. Exp 160, 10–3791. 10.3791/61345.
56. Dobin A, Davis CA, Schlesinger F, Drenkow J, Zaleski C, Jha S, Batut P, Chaisson M, and Gingeras TR (2013). STAR: ultrafast universal RNA-seq aligner. Bioinformatics 29, 15–21. 10.1093/bioinformatics/bts635. [PubMed: 23104886]
57. Trapnell C, Williams BA, Pertea G, Mortazavi A, Kwan G, van Baren MJ, Salzberg SL, Wold BJ, and Pachter L. (2010). Transcript assembly and quantification by RNA-Seq reveals unannotated transcripts and isoform switching during cell differentiation. Nat. Biotechnol 28, 511–515. 10.1038/nbt.1621. [PubMed: 20436464]
58. Ma H, Liang X, Chen Y, Pan K, Sun J, Wang H, Wang Q, Li Y, Zhao J, Li J, et al. (2011). Decreased expression of BATF2 is associated with a poor prognosis in hepatocellular carcinoma. Int. J. Cancer 128, 771–777. 10.1002/ijc.25407. [PubMed: 20473897]
59. Zhang Y, Liu T, Meyer CA, Eeckhoute J, Johnson DS, Bernstein BE, Nusbaum C, Myers RM, Brown M, Li W, and Liu XS (2008). Model-based analysis of ChIP-Seq (MACS). Genome Biol. 9, R137. 10.1186/gb-2008-9-9-r137. [PubMed: 18798982]

Highlights

- Astrocytes upregulate BATF2 in response to IFNγ
- BATF2 binds to chromatin sites upstream of IRF1 to regulate its expression in astrocytes
- BATF2-deficient mice exhibit exacerbated clinical experimental autoimmune encephalomyelitis
- The core of chronic active multiple sclerosis lesions is enriched for astrocytic BATF2

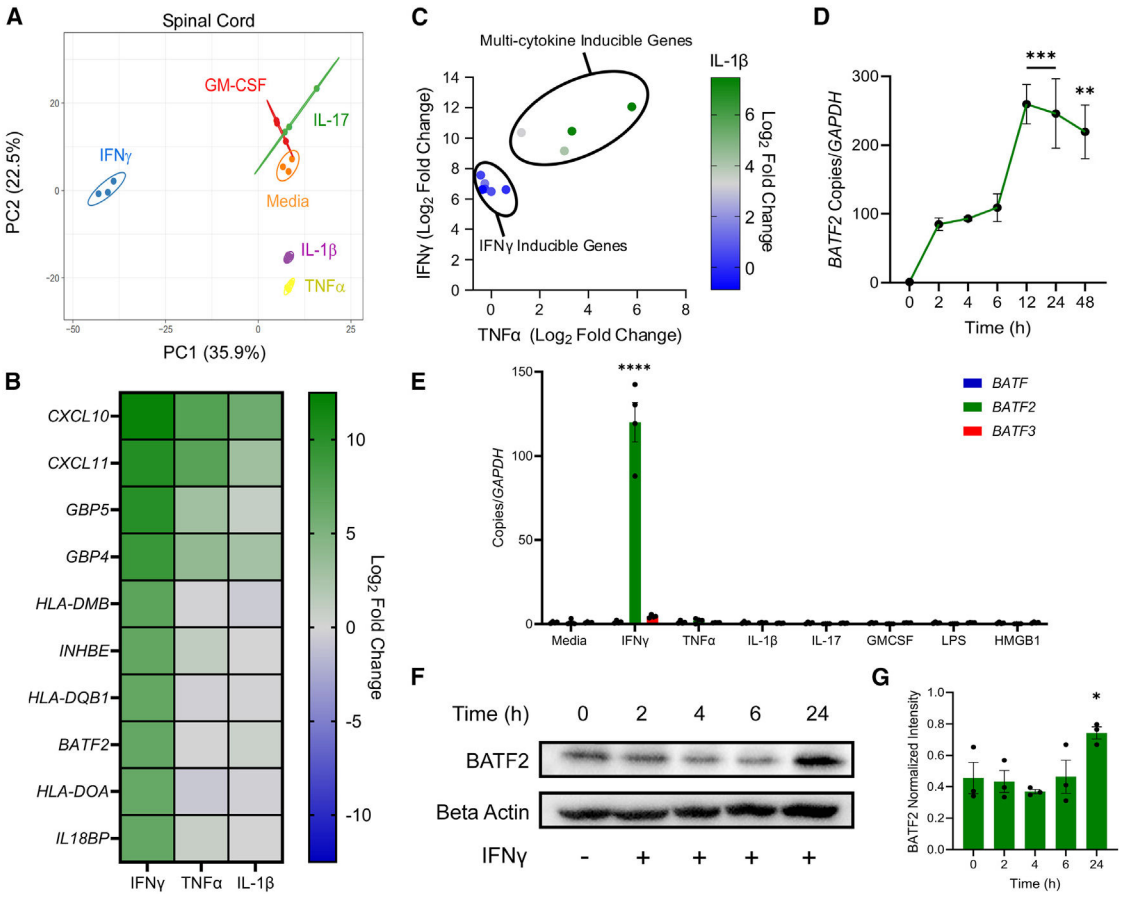

Figure 1. IFNγ signaling induces BATF2 expression in astrocytes

(A) PCA of RNA sequencing demonstrating distinct gene expression patterns of human spinal cord astrocytes treated with 10 ng/mL IFNγ, TNF-α, IL-1β, IL-17, GM-CSF, and media for 24 h.

(B) Heatmap of top upregulated genes in human spinal cord astrocytes treated with 10 ng/mL of IFNγ for 24 h compared to TNF-α and IL-1β treatments. Data represent log2 fold change compared to media from 3 independent samples.

(C) Top upregulated genes in human spinal cord astrocytes treated with 10 ng/mL IFNγ for 24 h compared to TNF-α and IL-1β treatments. Data represent the log2 fold change compared to media from 3 independent samples.

(D) *BATF2* transcript levels of human spinal cord astrocytes stimulated with 10 ng/mL IFNγ for 0–48 h. $^{**}p < 0.01$ and $^{***}p < 0.001$ compared to media-treated samples by one-way ANOVA. Data points represent mean ± SEM ($n = 3$).

(E) *BATF2* transcript levels of human spinal cord astrocytes treated with 10 ng/mL of various inflammatory stimuli for 24 h. $^{****}p < 0.0001$ compared to media-treated samples by two-way ANOVA. Bars represent mean ± SEM ($n = 4$).

(F) Representative western blot of whole-cell BATF2 protein levels in human spinal cord astrocytes treated with 10 ng/mL of IFNγ for 24 h.

(G) Quantification of whole-cell BATF2 protein levels in primary human spinal cord astrocytes shown in (F), normalized to β-actin expression. *$p < 0.05$ compared to media-treated samples by one-way ANOVA. Bars represent mean ± SEM ($n = 3$).

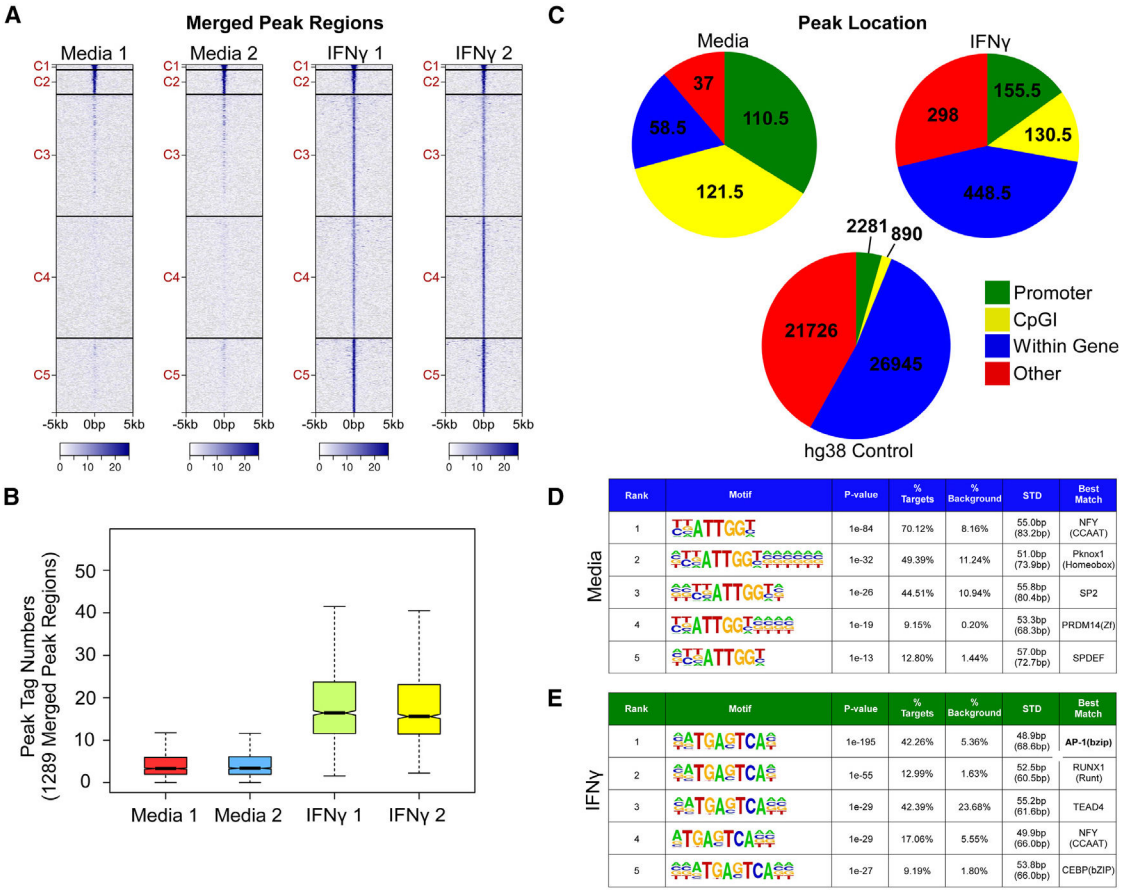

Figure 2. IFNγ increases DNA binding of BATF2 at inflammatory sites in astrocytes

(A) Merged peak region heatmap of BATF2 binding in human spinal cord astrocytes treated with 10 ng/mL IFNγ or media for 24 h. Scale bar indicates BATF2 binding events per merged region.

(B) Peak tag numbers of BATF2 binding events in 1,289 merged peak regions of human spinal cord astrocytes treated with 10 ng/mL IFNγ or media for 24 h.

(C) Peak location of BATF2 binding events in human spinal cord astrocytes treated with 10 ng/mL IFNγ or media for 24 h. hg38 binding events were used as an internal control. Data are the average peak locations between two independent samples per treatment.

(D and E) Top BATF2 binding motifs of media- and IFNγ-treated human spinal cord astrocytes.

Data shown in (A)–(E) are representative of two independent samples per treatment.

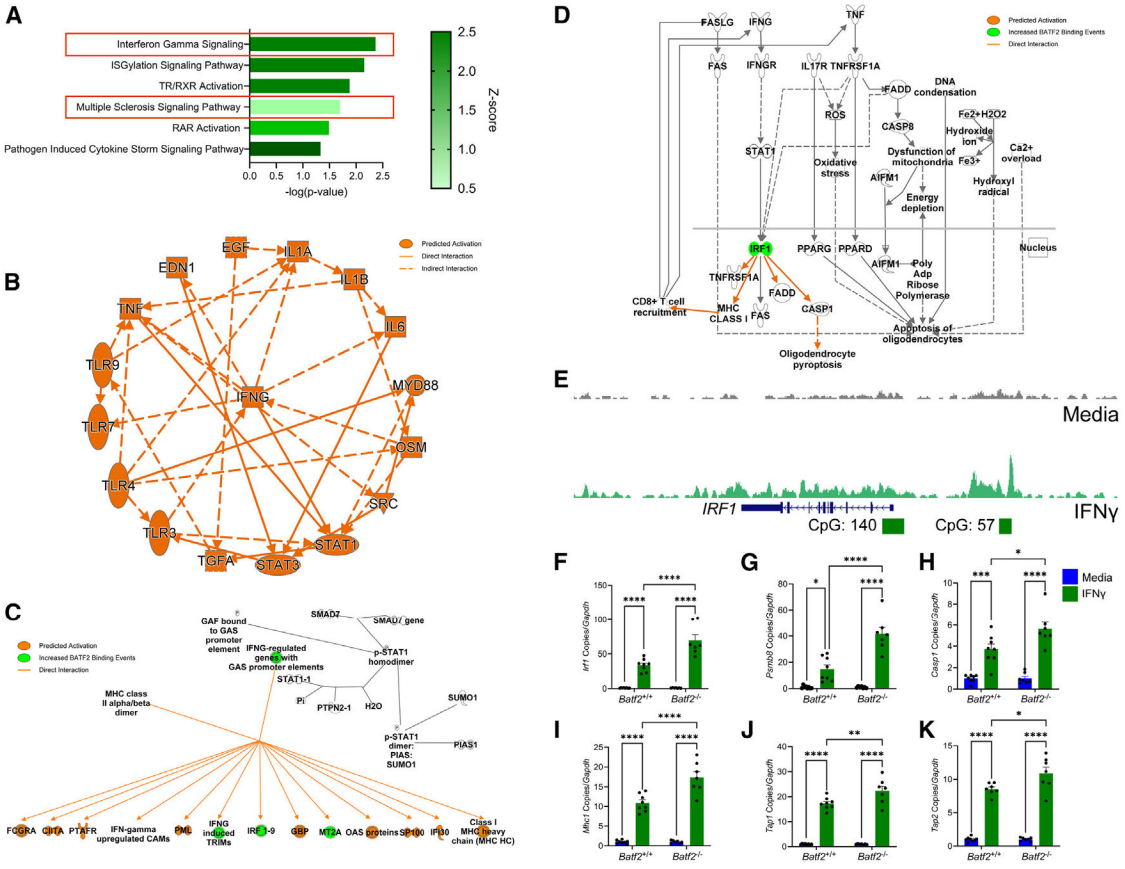

Figure 3. Astrocytic BATF2 suppresses the IRF1 signaling axis downstream of IFNγ

(A) Ingenuity pathway analysis of top regulated pathways by BATF2 in human spinal cord astrocytes stimulated with 10 ng/mL IFNγ for 24 h.

(B) Graphical summary of predicated targets regulated by BATF2 in human spinal cord astrocytes stimulated with 10 ng/mL IFNγ for 24 h.

(C) Adapted ingenuity pathway analysis: IFNγ signaling pathway from (A).

(D) Adapted ingenuity pathway analysis: multiple sclerosis signaling pathway from (A).

(E) Peak region counts of BATF2 binding events upstream of the *IRF1* gene locus and at CpG islands in human spinal cord astrocytes stimulated with 10 ng/mL IFNγ for 24 h (green) or media (gray).

(F–K) Quantification of *Irf1* and target gene transcript expression in $Batf2^{+/+}$ and $Batf2^{-/-}$ primary murine spinal cord astrocytes stimulated with media or 10 ng/mL IFNγ for 48 h. Data are representative of 2 independent experiments. Individual data points were normalized to the media average and are representative of individual mice. $*p < 0.05$, $**p < 0.01$, $***p < 0.001$, and $****p < 0.0001$ compared to media-treated samples by two-way ANOVA. Bars represent mean ± SEM ($n = 7$).

Data shown in (A)–(E) are representative of two independent samples per treatment.

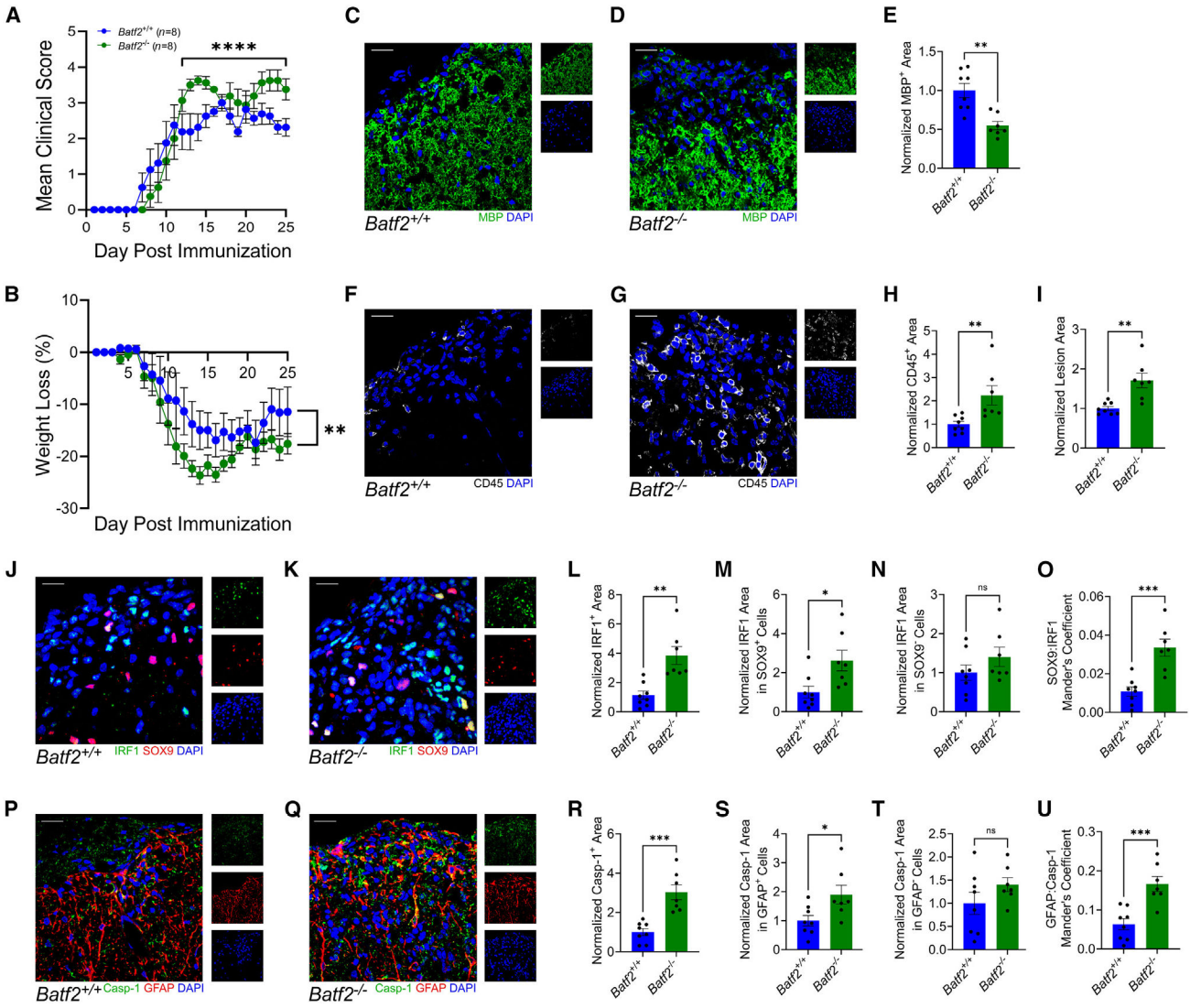

Figure 4. Loss of BATF2 exacerbates EAE and enhances IRF1 and caspase-1 expression *in vivo*

(A and B) EAE was induced in *Batf2*$^{-/-}$ and control mice. EAE (A) clinical course and (B) weights were blindly monitored. Data are a combination of 3 independent experiments and were analyzed using the Mann–Whitney *U* test for nonparametric data. $^{**}p < 0.01$ from day 2 and $^{****}p < 0.0001$. Data points represent mean ± SEM ($n = 8$ per genotype). 25 days post-immunization, mice were sacrificed, and the CNS tissue was cryopreserved for immunofluorescent analysis. Ventral white matter tracts of the lumbar spinal cord were imaged using confocal microscopy.

(C and D) Spinal cord tissue from (C) *Batf2*$^{+/+}$ and (D) *Batf2*$^{-/-}$ mice labeled for MBP and nuclei counterstained with DAPI. Scale bars, 20 μm.

(E) Quantification of MBP area normalized to the average of *Batf2*$^{+/+}$ control mice. $^{**}p < 0.01$ compared to *Batf2*$^{+/+}$ samples by two-tailed Student's t test. Bars represent mean ± SEM.

(F and G) Spinal cord tissue from (F) *Batf2*$^{+/+}$ and (G) *Batf2*$^{-/-}$ mice labeled for CD45 and nuclei counterstained with DAPI. Scale bars, 20 μm.

(H and I) Quantification of CD45 area and lesion area normalized to the average of *Batf2*$^{+/+}$ control mice. $^{**}p < 0.01$ compared to *Batf2*$^{+/+}$ samples by two-tailed Student's t test. Bars represent mean ± SEM.

(J and K) Spinal cord tissue from (J) *Batf2*$^{+/+}$ and (K) *Batf2*$^{-/-}$ mice labeled for IRF1, SOX9, and nuclei counterstained with DAPI. Scale bars, 20 μm.

(L–N) Quantification of IRF1 area normalized to the average of *Batf2*$^{+/+}$ control mice and IRF1 area in SOX9^{+} and SOX9^{-} cells normalized to lesion area and the average of *Batf2*$^{+/+}$ mice. $^{*}p < 0.05$ and $^{**}p < 0.01$ compared to *Batf2*$^{+/+}$ samples by two-tailed Student's t test. Bars represent mean ± SEM.

(O) Colocalization of SOX9 with IRF1 for *Batf2*$^{+/+}$ and *Batf2*$^{-/-}$ mice. $^{**}p < 0.01$ compared to *Batf2*$^{+/+}$ samples by two-tailed Student's t test. Bars represent mean ± SEM.

(P and Q) Spinal cord tissue from (N) *Batf2*$^{+/+}$ and (O) *Batf2*$^{-/-}$ mice labeled for caspase-1, GFAP, and nuclei counterstained with DAPI. Scale bars, 20 μm.

(R–T) Quantification of caspase-1 area normalized to the average of *Batf2*$^{+/+}$ control mice and caspase-1 area in GFAP^{+} and GFAP^{-} cells normalized to lesion area and the average of *Batf2*$^{+/+}$ mice. $^{*}p < 0.05$ and $^{***}p < 0.001$ compared to *Batf2*$^{+/+}$ samples by two-tailed Student's t test. Bars represent mean ± SEM.

(U) Colocalization of GFAP with caspase-1 for *Batf2*$^{+/+}$ and *Batf2*$^{-/-}$ mice. $^{***}p < 0.001$ compared to *Batf2*$^{+/+}$ samples by two-tailed Student's t test. Bars represent mean ± SEM.

Data in (C)–(U) are representative of 3 independent experiments and include mice that survived until endpoint at day 25 ($n = 8$ for *Batf2*$^{+/+}$, $n = 7$ for *Batf2*$^{-/-}$). Each data point is representative of an individual mouse.

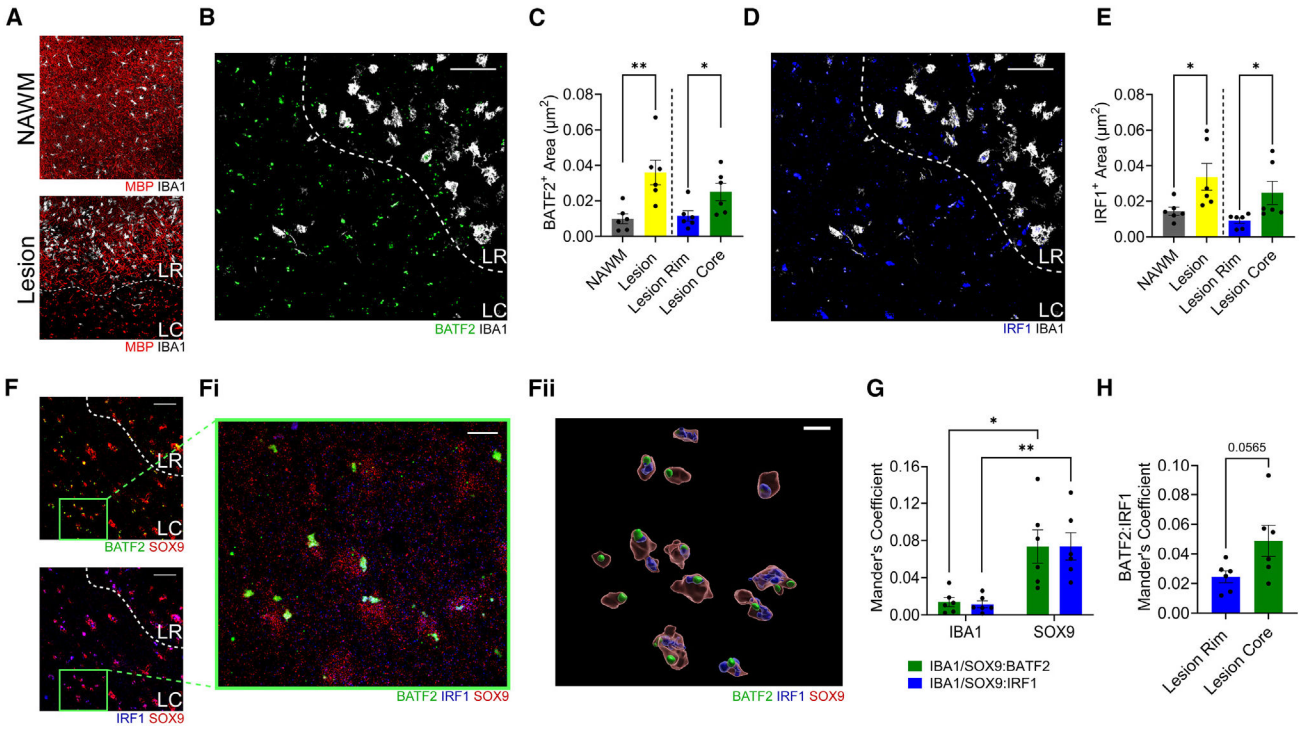

Figure 5. BATF2 is expressed by astrocytes in MS lesions and colocalizes with IRF1

(A) Human postmortem MS brain sections labeled for MBP and IBA1 to identify NAWM and chronic active lesions. Dotted line indicates the border of the LR and LC. Scale bars, 50 μm.

(B) Chronic active lesion labeled for BATF2 and IBA1. Dotted line indicates the border of the LR and LC. Scale bars, 50 μm.

(C) Quantification of BATF2 area. *$p < 0.05$ and **$p < 0.01$ by two-tailed Student's t test for each set of bars. Bars represent mean ± SEM.

(D) Chronic active lesion labeled for IRF1 and IBA1. Dotted line indicates the border of the LR and LC. Scale bars, 50μm.

(E) Quantification of IRF1 area. *$p < 0.05$ by two-tailed Student's *t* test for each set of bars. Bars represent mean ± SEM.

(F) Chronic active lesions labeled for BATF2 and SOX9 (top) and IRF1 and SOX9 (bottom). Dotted line indicates the border of the LR and LC. Scale bar, 50 μm. Green box indicates the area of interest within the LC. (Fi) High-magnification image of LC area of interest from (F) labeled for BATF2, IRF1, and SOX9. Scale bar, 10 μm. (Fii) Three-dimensional (3D) render of the high-magnification image from (Fi) labeled for BATF2, IRF1, and SOX9. Scale bar, 10 μm.

(G) Quantification of colocalization between SOX9 and IBA1 with BATF2 (green) and IRF1 (blue). *$p < 0.05$ and **$p < 0.01$ by one-way ANOVA for each set of bars. Bars represent mean ± SEM.

(H) Quantification of colocalization of BATF2 and IRF1 in the LR and LC. Data were analyzed by a two-tailed Student's t test. Bars represent mean ± SEM.

Data in (C), (E), (G), and (H) are representative of 2 independent experiments and include all patients represented in Table 1 ($n = 6$). Each data point is representative of an individual patient. LR, lesion rim; LC, lesion core.

Table 1.

Patient characteristics

Donor number	MS type	Age	Sex	Race	Final EDSS	Disease duration (years)
18	SPMS	45	M	White	7	36.0
115	SPMS	67	M	White	8	25.0
52	PPMS	27	M	White	8	1.8
17	SPMS	61	F	Black	9.5	35.3
20	PPMS	57	F	White	6.5	15.2
24	SPMS	48	F	White	9	27.1

EDSS, expanded disability status scale.

KEY RESOURCES TABLE

REAGENT or RESOURCE	SOURCE	IDENTIFIER
Antibodies		
BATF2 Polyclonal Antibody	Invitrogen	AB_2553927
BATF2 (1B11) mouse	Santa Cruz Biotechnology	AB_3676539
BATF2 Rabbit PolyAb	Proteintech	AB_2878285
SOX9 Antibody (CL0639)	Novus Biologicals	AB_3331802
IRF-1 (D5E4) XP® Rabbit mAb	Cell Signaling	AB_10949108
Caspase-1 Rabbit pAb	ABclonal	AB_2757485
PerCP/Cyanine5.5 anti-mouse CD45 Antibody	Biolegend	AB_893340
Recombinant Anti-Myelin Basic Protein antibody	Abcam	AB_305869
GFAP Polyclonal Antibody	Invitrogen	AB_1074620
GFAP Monoclonal Antibody (2.2B10)	Invitrogen	AB_2532994
Human SOX9 Antibody	R&D Systems	AB_2194160
Anti Iba1, Rabbit, SPICA Dye™ 594-conjugated	FujiFilm Wako	AB_3094950
beta Actin Loading Control Monoclonal Antibody (BA3R)	Invitrogen	AB_10979409
Goat anti-Rabbit IgG (H + L) Cross-Adsorbed Secondary Antibody, HRP	Invitrogen	AB_2536530
Alexa Fluor™ 405 goat anti-rabbit IgG (H + L)	Invitrogen	AB_2890548
Alexa Fluor™ 488 goat anti-rabbit IgG (H + L)	Invitrogen	AB_143165
Alexa Fluor™ 555 goat anti-rat IgG (H + L)	Invitrogen	AB_2535855
Alexa Fluor ™ 647 goat anti-chicken IgG (H + L)	Invitrogen	AB_2535866
Donkey anti-mouse IgG (H + L) Alexa Fluor™ Plus 647 highly cross-adsorbed	Invitrogen	AB_2762830
Alexa Fluor™ 488 donkey anti-goat IgG (H + L)	Invitrogen	AB_2534102
Chemicals, peptides, and recombinant proteins		
Recombinant Human IFN-γ	Peprotech	300–02
Recombinant Human TNF-α	Peprotech	300-01A
Recombinant Human IL-1β	Peprotech	200-01B
Recombinant Human IL-17A	Peprotech	200–17
Recombinant Human GM-CSF	Peprotech	300–03
Recombinant Murine IFN-γ	Peprotech	315–05
Dry Milk, Non-Fat, Molecular biology Grade	Lab Scientific bioKEMIX	M0841
Triton X-100	Fisher Scientific	BP151-100
Halt™ Protease Inhibitor Cocktail (100X)	ThermoFisher Scientific	87786
2-Mercaptoethanol	Sigma Aldrich	M6250-100mL
2X Laemmli Sample Buffer	BioRad	1610737
5M NaCl	Invitrogen	AM9760G
Ethylenediamine Tetraacetate Acid (EDTA)	Fisher Scientific	BP2482-500
Tris, 1.0M Buffer Soln., pH 7.4	ThermoFisher Scientific	J60202.K2
TBS-Tween-20 (10X) pH 7.4	Lerner Research Institute Cell Services	389M1000CUST
Novex WedgeWell 4–20% Tris-Glycine Gel	Invitrogen	XP04205BOX

REAGENT or RESOURCE	SOURCE	IDENTIFIER
10X Tris/Tricine/SDS Buffer	BioRad	1610744
10X Tris/Glycine Buffer	BioRad	1610734
Clarity Max Western ECL Substrate	BioRad	1705062
Tween 20	Sigma Aldrich	P9416-100mL
Glycine	Fisher Scientific	BP381-1
10% SDS	AccuGENE	51213
D-sucrose	Fisher Scientific	BP220-212
10X D-PBS	Lerner Research Institute Cell Services	123–1000
Paraformaldehyde 32% Solution, EM Grade	Electron Microscopy Services	15714
Tissue Plus O.C.T Compound	Fisher Healthcare	23-730-571
Methyl Alcohol	Cardinal Health	C4324
Prolong Gold antifade reagent	Invitrogen	P36930
Normal Goat Serum	Thomas Scientific	C978H52
Penicillin Streptomycin (10,000 U/mL)	Gibco	15140122
Fetal Bovine Serum Heat Inactivated (500mL)	Lerner Research Institute Cell Services	FBS-500 HI
DMEM (1X)	Lerner Research Institute Cell Services	11–500
Astrocyte Medium	ScienCell	1801
0.25% Trypsin EDTA	Lerner Research Institute Cell Services	589G100CUST
0.05% Trypsin EDTA	Lerner Research Institute Cell Services	521–500
Hooke Kits™ for EAE Induction in C57BL/6 Mice	Hooke Laboratories	EK2110
Pertussis toxin in glycerol	Hooke Laboratories	BT-0105
Critical commercial assays		
RNeasy Mini Kit	Qiagen	74106
Dnase I, Amplification Grade	ThermoFisher Scientific	18068015
TaqMan Reverse Transcription	Applied Biosystems	N8080234
Power SYBR Green PCR Master Mix	Applied Biosystems	4367659
Pierce BCA Protein Assay Kit	ThermoFisher Scientific	23227
Deposited data		
“RNA sequencing of cytokine-treated regional human astrocytes”	NCBI BioProject database/SRA	https://www.ncbi.nlm.nih.gov/bioproject/1217517
“Batf2 is a regulator of interferon gamma signaling in astrocytes during neuroinflammation”	NCBI GEO	https://www.ncbi.nlm.nih.gov/geo/query/acc.cgi?acc=GSE288440
Experimental models: Cell lines		
Human Astrocytes-Spinal Cord	ScienCell	1820
Experimental models: Organisms/strains		
C57BL/6NJ (B6N)	The Jackson Laboratories	IMSR_JAX:005304
B6.129S6(Cg)-Batf2tm1.1Kmm/WyokJ (BATF2 KO)	The Jackson Laboratories	IMSR_JAX:031903
Oligonucleotides		

REAGENT or RESOURCE	SOURCE	IDENTIFIER
Primer for Human *BATF* Forward: CCCAGGAGAAGTCAGGAAGG	This paper	N/A
Primer for Human *BATF* Reverse: CTTGTCCAGGCCTCTGTCTC	This paper	N/A
Primer for Human *BATF2* Forward: AGACCCCAAGGAGCAACA	Ma et al.[58]	N/A
Primer for Human *BATF2* Reverse: CAGGGCGAGGTTGTCTTT	Ma et al.[58]	N/A
Primer for Human *BATF3* Forward: CAGCGTCCTGCAGAGGAG	This paper	N/A
Primer for Human *BATF3* Reverse: GCTGGGCAGAGGAGTGTC	This paper	N/A
Primer for Human *GAPDH* Forward: GAAGGTGAAGGTCGGAGTC	Smith et al.[9,10]	N/A
Primer for Human *GAPDH* Reverse: GAAGATGGTGATGGGATTTC	Smith et al.[9,10]	N/A
Primer for Murine *Batf2* Forward: GCCCAGCGCAGCCGGCAGAA	This paper	N/A
Primer for Murine *Batf2* Reverse: CCAGCTCAGTCTGCAAGGCCT	This paper	N/A
Primer for Murine *Irf1* Forward: GACATTATACCAGATAGCACCAC	This paper	N/A
Primer for Murine *Irf1* Reverse: TCCCTTCCTCATCCTCGT	This paper	N/A
Primer for Murine *Psmb8* Forward: CCGCAGAGCTATTGCTTATGC	This paper	N/A
Primer for Murine *Psmb8* Reverse: TGTGGTACATGTTGACGACTC	This paper	N/A
Primer for Murine *Casp1* Forward: GAAGGCCCATATAGAGAAAGATTTTATTG	This paper	N/A
Primer for Murine *Casp1* Reverse: GACAGGATGTCTCCAAGACACATT	This paper	N/A
Primer for Murine *Mhc1* Forward: GCCTCCTCCGTCCACTGA	This paper	N/A
Primer for Murine *Mhc1* Reverse: GCCACCACAGCTCCAATGAT	This paper	N/A
Primer for Murine *Tap1* Forward: CGAGTGTCTCGGGAATGCTG	This paper	N/A
Primer for Murine *Tap1* Reverse: GTGAACTGAAGCTGGTAGAGAACGA	This paper	N/A
Primer for Murine *Tap2* Forward: CCCACGGGTCCTCATCCT	This paper	N/A
Primer for Murine *Tap2* Reverse: CAGTTCTGTAGGGCCTGTTCAC	This paper	N/A
Primer for Murine *Gapdh* Forward: GGCAAATTCAACGGCACAGT	Smith et al.[9,10]	N/A
Primer for Murine *Gapdh* Reverse: AGATGGTGATGGGCTTCCC	Smith et al.[9,10]	N/A
Software and algorithms		
ImageJ v1.52a	National Institutes of Health	https://imagej.net
Fiji v1.54f	ImageJ	https://imagej.net/software/fiji/downloads
TrimGalore! v0.4.2	Babraham Bioinformatics	https://www.bioinformatics.babraham.ac.uk/projects/trim_galore/
STAR aligner v2.5.3	Dobin et al.[56]	https://github.com/alexdobin/STAR
Cufflinks v2.2.1	Trapnell et al.[57]	http://cole-trapnell-lab.github.io/cufflinks/
MACS v2.1.0	Zhang et al.[59]	https://www.encodeproject.org/software/macs/
Graphpad Prism v10.1.2	GraphPad Software	https://www.graphpad.com
Microsoft Excel v2402	Microsoft	https://www.microsoft.com
Image Lab v6.1	BioRad	https://www.bio-rad.com
Ingenuity Pathway Analysis (IPA) v111725566	Qiagen	https://digitalinsights.qiagen.com/
Zen Lite v 3.8.99	Ziess	https://www.zeiss.com

REAGENT or RESOURCE	SOURCE	IDENTIFIER
QuantStudio Real-Time PCR Software v1.7.2	Applied Biosystems (Thermofisher Scientific)	https://www.thermofisher.com
Imaris v10.2.0	Oxford Instruments: Imaris	https://imaris.oxinst.com/